Building and Environment 269 (2025) 112395

Contents lists available at ScienceDirect

Building and Environment

journal homepage: www.elsevier.com/locate/buildenv

No "true" greenery: Deciphering the bias of satellite and street view imagery in urban greenery measurement

Yingjing Huang [a,b], Rohit Priyadarshi Sanatani [b], Chang Liu [b], Yuhao Kang [c], Fan Zhang [a], Yu Liu [a], Fabio Duarte [b,*], Carlo Ratti [b]

[a] Institute of Remote Sensing and Geographical Information System, School of Earth and Space Sciences, Peking University, Beijing, China
[b] Senseable City Lab, Massachusetts Institute of Technology, Cambridge, United States
[c] Department of Geography and the Environment, The University of Texas at Austin, Austin, United States

ARTICLE INFO

Dataset link: https://doi.org/10.5281/zenodo.13167483

Keywords:
Urban greenery
Street view imagery
Satellite imagery
Measurement bias

ABSTRACT

Urban greenery is a crucial element in building sustainable cities and communities. Despite the widespread use of satellite and street view imagery in monitoring urban greenery, there are significant discrepancies and biases in their measurement across different urban contexts. Currently, no literature systematically evaluates these biases on a global scale. This study utilizes the Normalized Difference Vegetation Index (NDVI) from satellite imagery and the Green View Index (GVI) from street view imagery to measure urban greenery in ten cities worldwide. By analyzing the distribution and visual differences of these indices, the study identifies eight factors causing measurement biases: distance-perspective limitation, single-profile constraint, access limitation, temporal data discrepancy, proximity amplification, vegetative wall effect, multi-layer greenery concealment, and noise. Moreover, a machine learning model is trained to estimate the bias risks of urban greenery measurement in urban areas. We find that bias in most cities primarily stem from an underestimation of GVI. Dubai and Seoul present fewer areas with overall bias risk, while Amsterdam, Johannesburg and Singapore present more such areas. Our findings provide a comprehensive understanding of the differences between the metrics and offer insights for urban green space management. They emphasize the importance of carefully selecting and integrating these measurements for specific urban tasks, as there is no "true" greenery.

1. Introduction

A more refined and accurate measurement of urban greenery is fundamental to building sustainable cities and communities. Urban greenery impacts residents' physical and mental well-being by promoting walkability and enhancing daily life [1,2]. It also contributes to improving air quality, enhancing biodiversity, and regulating urban heat [3,4]. Monitoring urban greenery at a large scale is essential for maintaining the health and functionality of urban green spaces, ensuring they provide long-term benefits to both people and the environment.

There are two main approaches to measuring urban greenery on a large scale: satellite imagery-based and street view imagery-based measurements. Over the past few decades, satellite imagery has consistently been used as a tool for greenery measurement due to its broad spatial coverage and convenient accessibility [5,6]. Remote sensing technology can use multispectral and hyperspectral imaging to capture electromagnetic spectrum information invisible to the human eye, such as infrared and ultraviolet. These multispectral images are useful for vegetation index calculation. Indices such as the Normalized Difference Vegetation Index (NDVI) [7] and the Leaf Area Index (LAI) [8] are widely used to quantify vegetation. Such indices support large-scale greenery measurement and tracking temporal changes [6,9]. Alternatively, street view imagery has emerged as a resource for urban greenery measurement in recent years [10]. Street view imagery is captured by ground-based imaging equipment, such as vehicle-mounted cameras [11,12]. Such images detail surface features like buildings, roads, and trees. One widely used metric for measuring urban greenery in street view imagery is the Green View Index (GVI), which quantifies the proportion of visually perceived green elements within the images [13]. Various studies have applied GVI as a proxy of urban greenery [14,15].

Despite the relevance of both satellite and street view imagery as valuable data sources for urban greenery mapping and analysis, they both have inherent limitations that prevent them from reflecting the "true" status of urban greenery. Satellite imagery offers a top-down view, making it impossible to capture vertical greenery such as vegetation walls (see Fig. 1(a)). In contrast, street view imagery

* Corresponding author.
E-mail address: fduarte@mit.edu (F. Duarte).

https://doi.org/10.1016/j.buildenv.2024.112395
Received 8 August 2024; Received in revised form 5 November 2024; Accepted 1 December 2024
Available online 20 December 2024

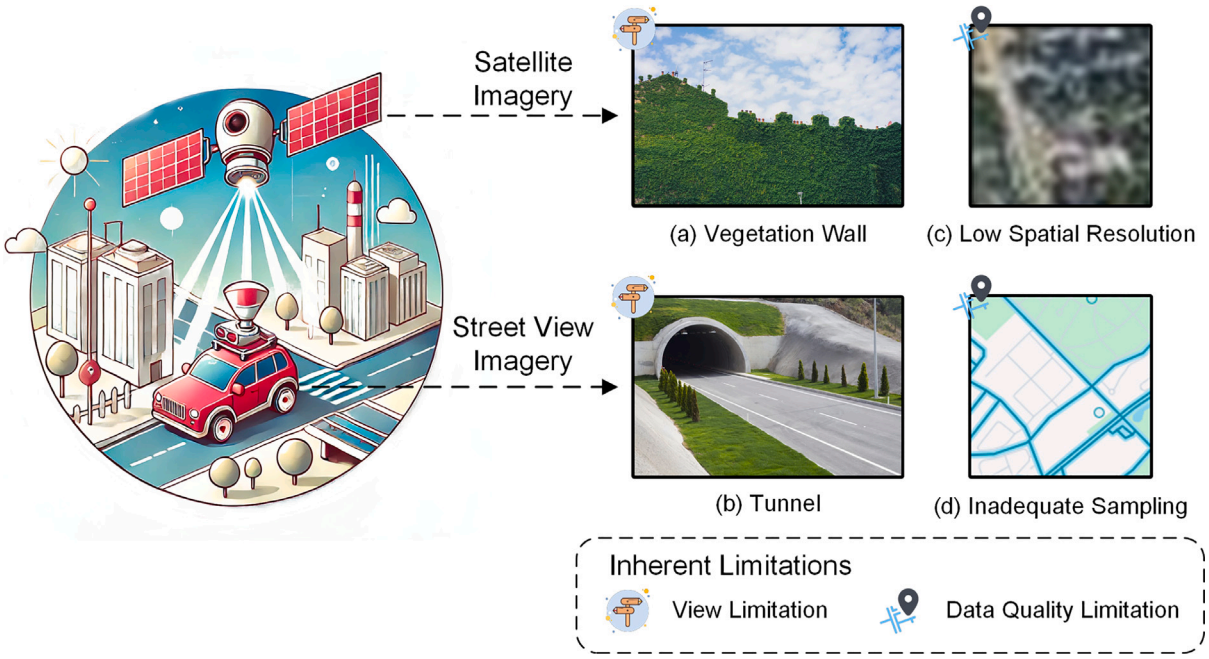

Fig. 1. Inherent limitations of satellite and street view imagery. (a) Vegetation wall; (b) Tunnel; (c) satellite imagery with 10-m spatial resolution; (d) Street view sampling distribution.
Source: ChatGPT, Unsplash, Google Earth, and Google Maps.

allows observation of the vertical urban environment, but they are easily obstructed by tunnels or large trucks (see Fig. 1(b)). Moreover, in terms of data quality, satellite imagery typically has lower spatial resolution, making it difficult to distinguish small greenery elements on the ground. On the other hand, street view imagery is not uniformly distributed, with some internal roads and public pathways suffering from inadequate sampling. Such inherent limitations influence not only the accuracy of greenery measurements but also subsequent analyses and interpretations [16,17], potentially resulting in misleading conclusions.

Although existing literature recognizes potential biases in satellite and street view-based measurements of urban greenery across different urban environments, these biases and their causes have not been systematically discussed. For example, [18,19] both noted that satellite-based measurements often miss vertical greenery, such as individual trees or other green elements, particularly in densely urbanized areas [20,21]. [18] suggested using an NDVI:GVI ratio as an indicator of vertical greenery in such scenarios to address this type of bias. Regarding street view measurements, [20] found that the density of street view sampling points also affects the measurement of urban greenery, leading to the proposal of a Standardized Green View Index (sGVI) that calculates the GVI of an area weighted by the locations of the sampling points. Additionally, there is extensive literature discussing the correlation between NDVI and GVI, with most studies finding a moderate correlation, with correlation coefficients ranging approximately from 0.40 to 0.76 [18,21,22]. These studies provide valuable insights into the quantitative differences between the two greenery measurement methods, but the qualitative factors behind them are typically discussed through local findings combined with specific research questions. The subtle nuances of these differences and their underlying factors remain to be fully understood. Furthermore, most past studies have been conducted on local datasets, and their results may not be generalizable to other regions [23,24]. Therefore, there is a need to systematically examine and categorize the causal factors behind the differences between satellite and street view-based measurements on a global scale, providing directions for more sensitively interpreting these indices.

To address this research gap, this study computed the values of NDVI and GVI across ten cities worldwide, characterized by diverse geographical locations and climates, and conducted a quantitative analysis of the differences and trends between them. Based on the characteristics of these differences, we identified eight main factors that could potentially cause biases. Furthermore, we trained a machine learning model to assess the risk of bias in greenery measurements based on satellite and street view data, allowing for an assessment of greenery measurement bias risks across broader urban areas. Through this qualitative and quantitative analysis of greenery measurements, we provide deep insights for future precise measurements of urban greenery and related research fields. This study not only enhances our understanding of urban greenery measurement techniques but also reveals the effectiveness and limitations of different measurement tools applied in various global cities.

2. Methods

Fig. 2 illustrates the workflow of this study, which comprises five parts: data collection, greenery extraction, difference analysis, bias identification, and bias quantification. Initially, we collected Sentinel-2 satellite imagery and Google Street View imagery across ten global cities. Subsequently, greenery was extracted from these two distinct data sources: NDVI was calculated using raster calculation from satellite images, and GVI was derived using semantic segmentation models from street view images. These measurements were then aggregated at a grid spatial scale to represent urban greenery as NDVI and GVI values. Through statistical and spatial analyses, we identified the global differences between NDVI and GVI. Finally, we identified the types of biases and quantitatively estimated the risk of these biases by constructing a machine-learning model.

2.1. Data collection

We selected ten metropolitan areas as our study areas: Amsterdam, Barcelona, Boston-Cambridge-Medford-Newton (Boston), Buenos Aires, Dubai-Sharjah (Dubai), Johannesburg, Los Angeles, Melbourne, Seoul, and Singapore. These areas were chosen to represent a wide array of global climates, ecosystems, cultures, and urban environments, thereby

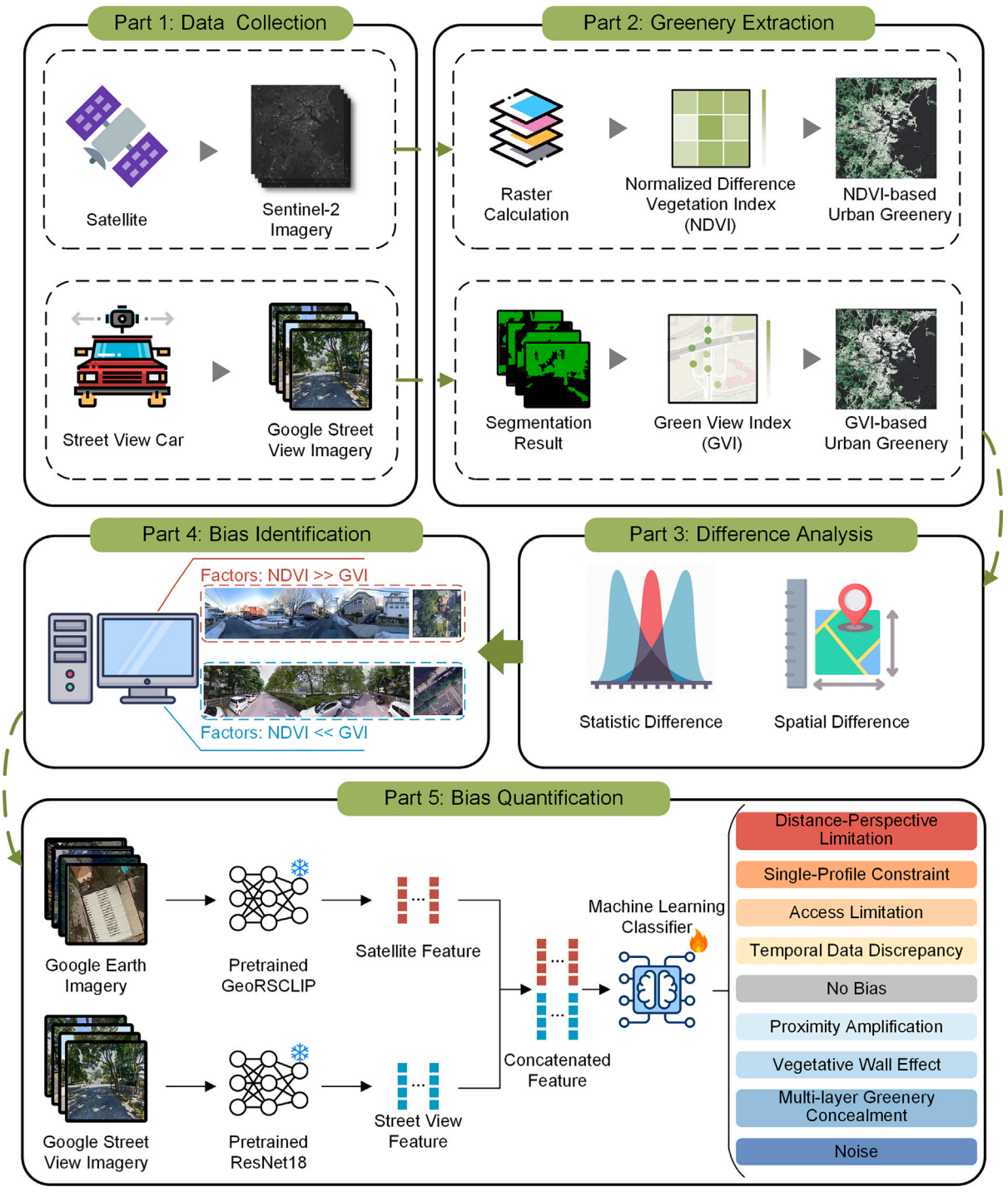

Fig. 2. The research workflow.

offering a comprehensive understanding of disparity patterns in urban greenery detection across various geographical contexts.

In alignment with methodologies in existing literature, the data sources used in this paper are:

Satellite imagery. The European Space Agency launched the Sentinel-2 constellation, comprising twin satellites, which offers 13 spectral bands with high resolution. Notably, four of these bands, namely red (665 nm), green (560 nm), blue (490 nm), and visible and near-infrared (842 nm), have a spatial resolution of 10 m. We selected Sentinel-2 as it offers higher spatial resolutions, which surpasses other open-source satellite datasets such as MODIS and Landsat series satellites. The collection of Sentinel-2 images was conducted across ten cities. To ensure data reliability, the Level-2 A product, containing atmospherically corrected surface reflectance images, was selected from the various level products of Sentinel-2. To facilitate more accurate calculations of NDVI [25]. Due to the high temporal resolution offered by remote sensing technologies, urban greenery measurements are commonly conducted utilizing imagery acquired during the most recent cloud-free summer period. Since some cities may consist of multiple patches, these cities might have data from multiple dates. Detailed collection dates are presented in Table 1.

Street view imagery. To obtain street view imagery, the road network data for each city was acquired from OpenStreetMap by the OSMnx library [26]. Subsequently, query points were established along

Table 1
Data description of each of the metropolitan areas.

Metropolitan area	Country	Collection date of Satellite imagery	# of Street view images
Amsterdam	Netherlands	June 09, 2023; June 14, 2023	488,956
Barcelona	Spain	April 02, 2023	430,240
Boston	United States	April 02, 2023; May 29, 2023; June 11, 2023	467,836
Buenos Aires	Argentina	January 23, 2023	265,956
Dubai	United Arab Emirates	June 12, 2023	700,892
Johannesburg	South Africa	January 11, 2023	596,204
Los Angeles	United States	March 24, 2023	880,548
Melbourne	Australia	January 27, 2023	915,860
Seoul	South Korea	June 16, 2023	586,094
Singapore	Singapore	March 16, 2023	712,892

the road network, with a regular interval of 15 m. The Google Street View (GSV) Application Programming Interface (API) was then employed to retrieve and download street view images. A substantial collection of street view images, totaling 3,681,364, was successfully obtained from 920,341 unique locations across the ten cities. Each location in the dataset includes a unique point ID, year and month of image capture, and its corresponding coordinates, accompanied by four street view images corresponding to the cardinal directions, namely North, East, South, and West. The data used in this study comes from the latest version of Google Street View as of May 2023. However, due to varying update frequencies for each sampling point, the images may have been captured at different times, ranging from as recent as one month ago to as far back as ten years.

2.2. Greenery extraction

For satellite imagery, we used the Normalized Difference Vegetation Index (NDVI), a well-established measure initially by Rouse et al. [7] for monitoring ground-level vegetation. The NDVI was calculated with 10-m resolution data of Sentinel-2. It is defined as:

$$NDVI = \frac{R_{nir} - R_{red}}{R_{nir} + R_{red}} \quad (1)$$

where R_{nir} and R_{red} represent the spectral bands at near-infrared (842 nm) and red (665 nm), respectively. Such a unit-less index is normalized to yield values ranging between −1 and 1, wherein a value of 1 corresponds to full vegetation coverage. Considering that negative values commonly indicate the presence of clouds and water [23], such values were adjusted to 0, implying an absence of greenery. To facilitate comparison with street view-based measurements, NDVI values were aggregated according to grid units at different scales.

For street view imagery, we used the Dense Prediction Transformer (DPT) [27] model for semantic segmentation, as it has been validated through multiple studies [28]. The DPT model used in this study was pre-trained on the ADE20K dataset [29] and achieved a pixel-level segmentation accuracy of 83.11% and a mean Intersection over Union (mIoU) of 49.02%, outperforming mainstream models such as Deeplabv3 [27]. It categorizes each pixel into one of 150 semantic classes. The calculation of GVI focuses on identifying greenery elements present in the images. In this study, we utilized five greenery classes: "tree", "grass", "plant", "palm tree", and "field". Although "field" is not traditionally considered a greenery element, we included it to align with the NDVI calculation. Moreover, due to the distribution limitations of street view data, our study area is predominantly urban, where the "field" category is rarely observed. As a result, its impact on the overall findings is minimal. The GVI in this study was defined consistent with existing literature [13,30] as the ratio of greenery pixels to the total pixels in each image. It is defined as:

$$GVI = \frac{N_{greenery}}{N_{total}} \quad (2)$$

where $N_{greenery}$ represents the number of pixels of greenery classes, and N_{total} represents the number of total pixels. The GVI values fall within the range of 0 to 1, where a value of 1 indicates full vegetation coverage and a value of 0 signifies the absence of greenery in the image.

Both NDVI and GVI metrics range from 0 to 1, with higher values denoting greater vegetation coverage. To maintain consistency in spatial scales when comparing NDVI and GVI, we aggregated NDVI and GVI values into 100-m grids. The grids that lack street view sampling points are excluded from further analysis. It should be noted that grids with only a small amount of street view sampling points were also included in the analysis. This is because the variation in urban environments makes it difficult to establish a uniform and reasonable threshold to determine whether the data quantity is sufficient to represent the grid. Additionally, we believe that sparse sampling points may be one of the factors contributing to bias.

2.3. Difference analysis

This study compares the differences between NDVI and GVI through both statistical and spatial analyses. In the statistical analysis, we focus on the distribution of the quantiles of NDVI and GVI. For the spatial analysis, we employ hotspot analysis to explore the spatial distribution patterns of the differences. Initially, we perform min–max normalization on the values of NDVI and GVI to ensure that both are compared on the same scale. Subsequently, we conduct hotspot analysis on the normalized differences using the Getis–Ord Gi* statistic [31], a method widely used to reveal localized spatial clustering patterns. This granular approach allows us to precisely identify significant hot and cold spots, uncovering critical clusters where NDVI is significantly higher than GVI, or vice versa. The Getis–Ord Gi* statistical analysis was conducted using ArcGIS Pro 3.0, with the conceptualization of spatial relationships set to inverse distance squared and the Euclidean distance method applied.

2.4. Bias identification

For identification of bias types, we first isolated locations which presented the highest standardized difference between NDVI and GVI. These were grouped in two categories — locations where NDVI exceeded GVI and locations where GVI exceeded NDVI. For both categories, a qualitative visual analysis was undertaken by the authors and 4 primary causal factors behind the differences were identified and summarized for each group.

We subsequently developed a dataset annotated with multiple types of bias. Specifically, we divided the grid data of each city into 10 groups based on the standardized differences between NDVI and GVI. For each group, we randomly selected 20 samples, resulting in a total of 2000 samples. Each sample includes Sentinel-2 satellite imagery, high-resolution Google Earth imagery, and several street view images corresponding to the grid. We annotated the dominant bias factor for each sample, with the addition of a "no bias" category. Samples where the bias factors w composed of multiple factors were excluded. The final dataset contains 1897 valid samples, which we believe clearly represent the characteristics of different bias types. The annotation of these samples was accomplished using the open-source software

Label Studio.[1] This process not only aids in understanding the specific causes of biases but also provides a data foundation for further machine learning analysis.

2.5. Bias quantification

To quantitatively analyze bias types in urban areas, we trained a machine learning model using the bias-annotated dataset. Specifically, two-thirds of the data were randomly selected as the training set, while the remaining one-third was used as the test set. As illustrated in Fig. 2, to precisely analyze the material features and structures of urban spaces, we employed 0.6-m resolution RGB Google Earth images in place of 10-m resolution multispectral Sentinel-2 imagery. We optimized the model's performance on a small sample set by extracting features from satellite and street view images using two pretrained models. The satellite image features were extracted using the GeoRSCLIP model, pretrained on the RS5M dataset [32], while the street view image features were extracted using the ResNet18 model, pretrained on the Places365 dataset [33]. Both models were pretrained on large-scale image datasets and are widely used for urban scene recognition. Their deep feature representations capture the underlying semantic understanding of urban environments, making them highly suitable as feature extractors for our study.

Feature extraction resulted in a 512-dimensional feature vector for each grid from satellite images and multiple 512-dimensional feature vectors from street view images. By averaging the street view image features, we obtained a representative vector for each grid. These features were then concatenated, forming a 1024-dimensional vector for each grid. Utilizing these feature vectors, we trained a Support Vector Machine (SVM) model to classify bias types, setting the regularization parameter at 100 and using the Radial Basis Function (RBF) kernel. Due to the imbalanced distribution of samples across categories, we applied class weighting to ensure the model appropriately adjusted for the differing representation of each bias type. All feature extraction and model training were conducted using Python's PyTorch and scikit-learn libraries.

3. Results

3.1. Differences between satellite-based and street view-based urban greenery

NDVI and GVI serve as representative indices for satellite-based and street view-based urban greenery, respectively. The choice of a 100-m grid was made to ensure both data representativeness and measurement accuracy. As a finer spatial resolution, a 100-m grid effectively illustrates the characteristics and differences of urban greenery as measured from satellite and street view perspectives.

Fig. 3(a) illustrates the statistical distribution of NDVI and GVI across various cities, demonstrating a general alignment in their representation of overall urban greenery. For instance, cities like Dubai and Seoul exhibit generally low greenery, whereas Johannesburg, Amsterdam, and Boston display relatively high levels of urban greenery. Despite this consistency, there are notable differences between NDVI and GVI. Specifically, in cities such as Buenos Aires, Singapore, and Melbourne, GVI values are significantly higher than those of NDVI. For instance, in Singapore, the median GVI value is 0.2465, which is 65% higher than the median NDVI value of 0.1488.

To enhance the comparison of NDVI and GVI differences at a finer granularity, we standardized the NDVI and GVI data for each city and conducted a hot and cold spot analysis based on these normalized differences. The results are depicted in Fig. 3(b). In this figure, hot spots represent areas where GVI is significantly lower than NDVI, while cold spots indicate regions where GVI substantially exceeds NDVI. The analysis reveals that most cities display a network-like distribution of hot spots, with Boston exhibiting a patchy distribution. As for cold spots, while most cities show sporadic distributions, in Los Angeles and Singapore, these areas are predominantly concentrated within urban centers.

3.2. Factors contributing to measurement biases

Statistical and geographical analyses both indicate significant differences between NDVI and GVI in measuring urban greenery, particularly at a fine-grained level. These differences are closely associated with the methods of data collection and the physical environment of the cities. To better understand the reasons behind the differences between NDVI and GVI, we visually annotated the primary factors contributing to these discrepancies. The Sentinel-2 data used for calculating NDVI has a resolution of 10 m, which limits its ability to distinguish elements in 100-m grids. Consequently, in this section, we utilized Google Satellite Imagery with a higher resolution of 0.6 meters to enhance our understanding of the visual differences.

Four primary factors are annotated, which are responsible for underestimating urban greenery in street view imagery: distance-perspective limitation, single-profile constraint, access limitation, and temporal data discrepancy.

Distance-Perspective Limitation: Street view imagery's depiction of distant vegetation suffers from pixel representation limitation due to visual perspective, an issue not present in satellite images. Fig. 4(a) illustrates the challenge, showcasing how distant vegetation in Amsterdam becomes indistinct, especially when compared with fields or grasslands (see Fig. 4(b)). This limitation becomes more apparent in areas with broader roads, making the vegetation near these roads seem more distant to the camera.

Single-Profile Constraint: At forest boundaries adjacent to roads, street view imagery often captures merely one side of the forest, especially in the absence of internal roads, as demonstrated in Fig. 4(c). In contrast, satellite imagery, with its overhead view, provides a more comprehensive portrayal of the forest, underscoring the restricted perspective of street view.

Access Limitation: Green spaces that are obstructed by the linear perspective of street view or are inaccessible. Examples include road structures such as overpasses and tunnels and areas with access limitations, such as parks, schools, and private gardens. Fig. 4(d) provides an example, highlighting the inability of street view imagery, taken from an overpass, to capture the greenery at ground level, a challenge not present in satellite imagery. Furthermore, the exclusion of private gardens from the public collection in street view imagery, as illustrated in Fig. 4(e), adds to the underestimation.

Temporal Data Discrepancy: The infrequency of updates in street view imagery can misrepresent real-world greenery, especially when considering seasonal shifts and changes in land use. For example, in Boston, the climatic conditions combined with certain tree species result in seasonal leaf fall or snow cover, causing a marked underrepresentation of greenery in street view images taken during fall and winter, as shown in Fig. 4(f). Satellite imagery, with its more frequent updates, often sidesteps this issue. Similarly, recognizing temporal land use changes promptly is imperative. A construction zone in Dubai depicted in street view, as presented in Fig. 4(g), is shown to be a meadow in the most recent satellite image.

Another four factors are detected, which render street view imagery greener than satellite imagery: proximity amplification, vegetative wall effect, multi-layer greenery concealment, and noise.

Proximity Amplification: In street view imagery, the perception of nearby vegetation is often exaggerated due to the intrinsic properties of visual perspective. Such vegetation occupies a substantial portion of the image, as demonstrated in Fig. 5(a). A tree prominently displayed

[1] https://labelstud.io/

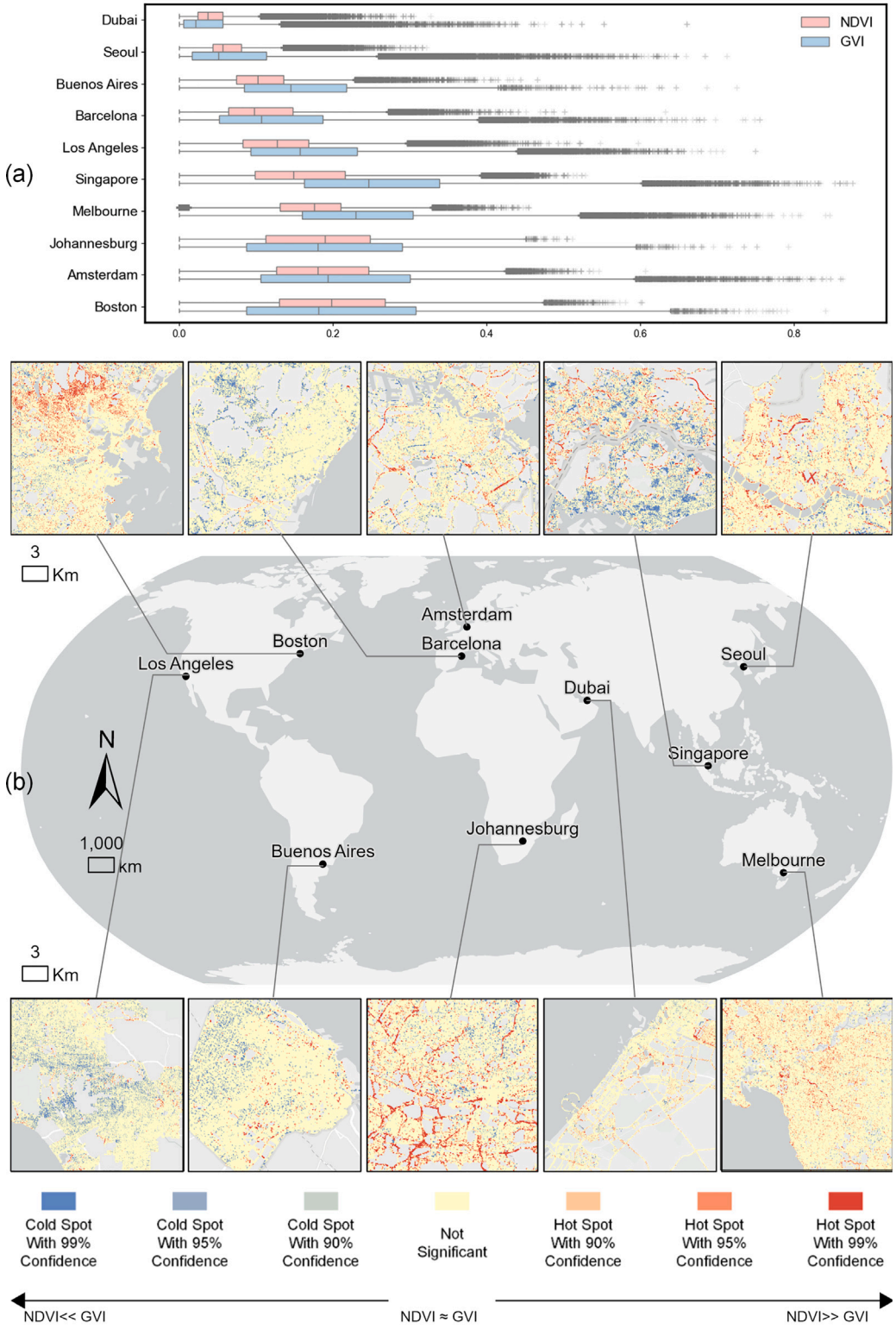

Fig. 3. Differences between NDVI and GVI. (a) Statistical distribution of NDVI and GVI across ten cities. The box shows the interquartile range (IQR), with the median represented by a line inside the box. Whiskers extend to 1.5 times the IQR, and outliers are plotted as individual points. The cities are arranged in order of their mean NDVI values; (b) Spatial distribution of hot and cold spots. Hot spots denote areas where GVI is significantly lower than NDVI, and cold spots signify regions where GVI substantially exceeds NDVI.

in the street view might be one of the few green elements in the surrounding environment. It is essential to note that a significant portion of such areas, as seen in Fig. 5(a), may be non-green spaces such as parking lots. It highlights how the potential for uneven distribution of street view imagery can exaggerate the presence of greenery in urban environments that have sparse vegetation.

Vegetative Wall Effect: Vertical vegetation features can present a continuous green wall. This is exemplified in two forms: the vine wall

Fig. 4. Four factors of satellite imagery being greener than street view imagery. (a)–(b) Distance-perspective limitation; (c) Single-profile constraint; (d)–(e) Access limitation; (f)–(g) Temporal data discrepancy.

and the tree wall. Fig. 5(b) showcases the vine wall in street view imagery, a green facade alongside roads. In contrast, satellite imagery may obscure or diminish such vertical features. Tree species with thick canopies, when densely planted, can create a tree wall, which might appear merely as a thin green strip in satellite views, as depicted in Fig. 5(c).

Multi-layer Greenery Concealment: Diverse vegetation types, such as trees, shrubs, and grasses, are visually discernible in profile views, as in street view imagery. Satellite imagery, on the other hand, predominantly captures the uppermost vegetation layer. This leads to potential underrepresentation, as seen in Fig. 5(d), where under-canopy shrubs visible in street view are absent in the satellite counterpart.

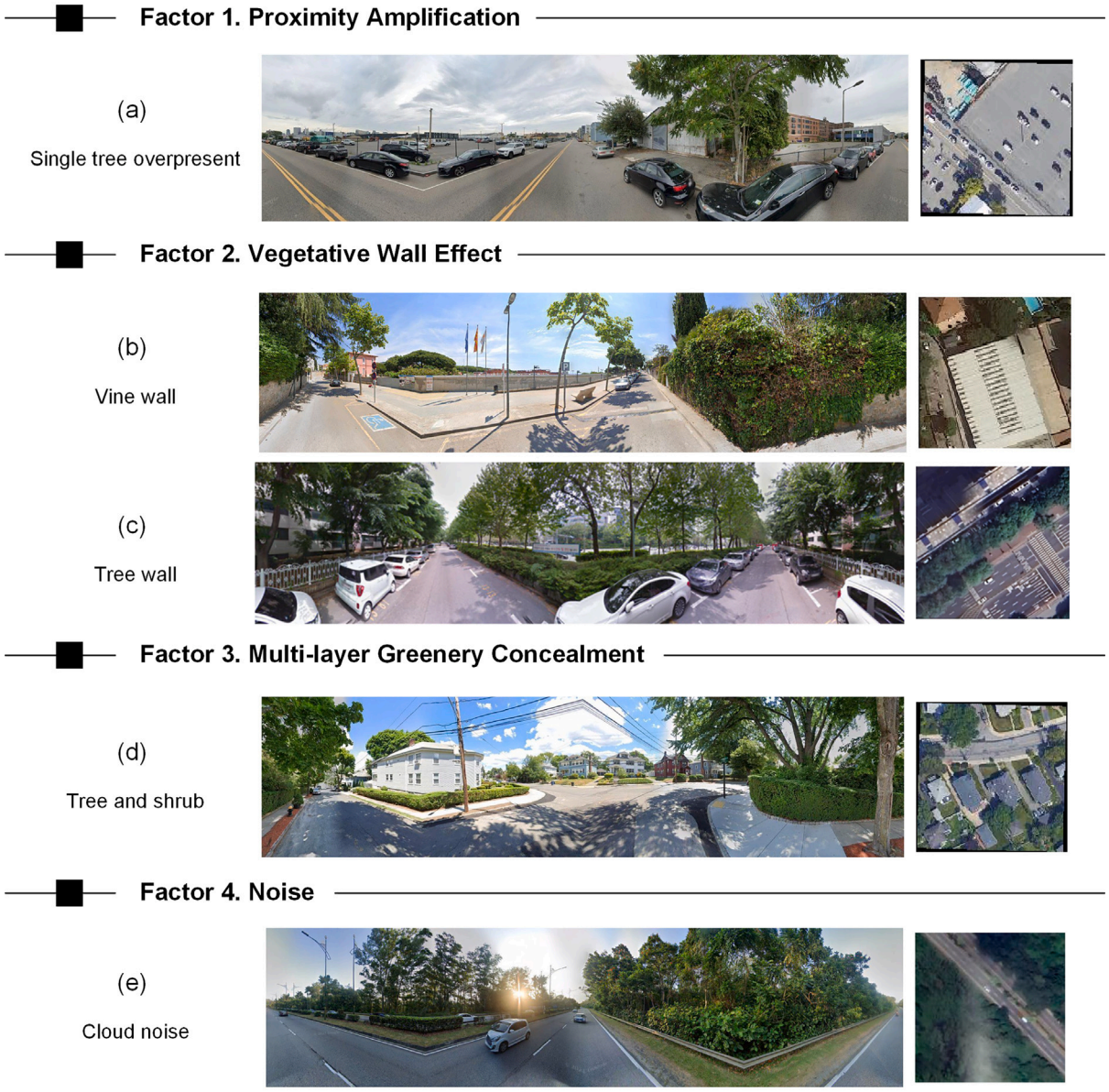

Fig. 5. Four factors of street view imagery being greener than satellite imagery. (a) Proximity amplification; (b)–(c) Vegetative wall effect; (d) Multi-layer greenery concealment; (e) Noise.

Noise: Interference during satellite image acquisition, notably cloud cover, can mask underlying vegetation. Fig. 5(e) portrays a region with substantial forest cover. However, the satellite-derived NDVI value is considerably lower than the GVI, suggesting an obstruction in image acquisition. Detailed examination of the Sentinel-2 image reveals persistent cloud cover. Even with advanced data processing, certain clouds remain visible in the Google Satellite imagery, hinting at possible perennial cloud presence, thus influencing accurate greenery quantification.

Table 2
Categories of the bias-annotated dataset.

Category	# of samples
Distance-Perspective Limitation	315
Single-Profile Constraint	81
Access Limitation	493
Temporal Data Discrepancy	152
No Bias	753
Proximity Amplification	47
Vegetative Wall Effect	22
Multi-layer Greenery Concealment	30
Noise	4

3.3. Quantification of bias types

To explore the bias risks associated with urban greenery, we created a dataset annotated with various types of biases. This dataset includes eight distinct bias factors as well as a "no bias" category, with the distribution of these categories presented in Table 2. We then trained a machine learning model to identify these bias types. The model achieved an overall accuracy of 63.16%, a weighted average F1 score of 0.62, and a weighted average recall of 0.63. Using this model, we can estimate the bias risk of the whole urban area.

We analyzed and compared the density distributions of NDVI and GVI across different predicted bias types, as shown in Fig. 6. Most bias types exhibit significant differences in the density peaks of NDVI and GVI. For example, the GVI distribution in the single-profile constraint

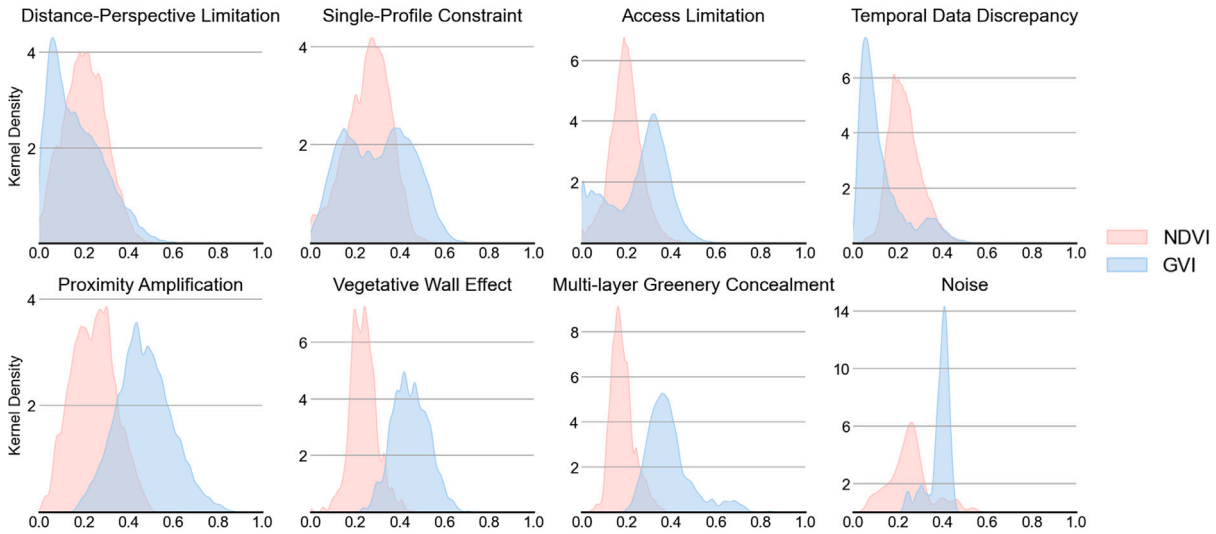

Fig. 6. Kernel density distributions of NDVI and GVI in different bias types.

is relatively dispersed. This is likely due to the diversity of scenes that lead to this bias, such as forest edges, where the visibility of vegetation adjacent to tree walls has minimal impact on the occurrence of this bias, resulting in a more diffuse distribution. Overall, the distribution patterns of most bias types align with our assumptions regarding the differences between NDVI and GVI. However, in the case of the access limitation, GVI shows a higher overall density compared to NDVI, which deviates from our anticipated characterization of this bias. This discrepancy may arise from the complexity of this type of scene, which not only involves physically inaccessible areas, such as beneath overpasses, but also legally restricted spaces, such as private gardens. These factors make it challenging for the machine learning model to fully capture the intricacies of this bias. In Section 4.3, we further discuss the limitations of the machine learning model; nonetheless, it effectively captures certain characteristics of bias risks.

Estimation results for bias risks across ten cities are presented in Fig. 7(a). It is apparent that bias in all cities primarily stems from the underestimation of GVI, with a notable exception in Barcelona where a significant proportion of bias is due to the underestimation of NDVI. Dubai and Seoul exhibit relatively fewer areas with bias risk, with total proportions of only 0.0220 and 0.0234, respectively. In contrast, Amsterdam, Johannesburg, and Singapore show slightly higher proportions of areas at risk, with total proportions of 0.1438, 0.1448, and 0.1453, respectively. Additionally, the predominant type of bias varies by city; for instance, Melbourne mainly faces issues due to access limitations, Boston due to temporal data discrepancy, and Amsterdam due to distance-perspective limitations.

Figs. 7(b), (c), and (d) depict the spatial distribution of bias types in Boston, Amsterdam, and Barcelona, respectively. In Boston, most of the northern regions are affected by temporal data discrepancies, while the highway areas in Amsterdam prominently feature distance-perspective limitations. Similarly, Barcelona faces distance-perspective limitations, but certain areas in the northwest and southwest also exhibit concentrated risks of proximity amplification bias.

4. Discussion

4.1. No true Greenery

This paper systematically identifies eight principal factors contributing to bias from a global perspective: distance-perspective limitations, single-profile constraints, access restrictions, temporal data discrepancies, proximity amplification effects, vegetative wall effects, multi-layered greenery concealment, and noise. We have quantitatively estimated the bias risks prevalent across all urban areas. It is important to note that while we have identified the primary factors causing biases in these regions, multiple factors may interact, leading to a greater overall bias or compensating for one another to reduce the apparent bias. For instance, an area may simultaneously exhibit access limitations and vegetative wall effects, whose combined impact might minimize the differences between the NDVI and GVI measurements.

These biases are largely attributable to the methods and characteristics of data collection. With the ongoing advancement of technology, it is hoped that these biases could be alleviated or even resolved to some extent. Our findings indicate that most biases stem from the underestimation of GVI. In some areas captured by street view imagery, the spatial resolution may be low and the sampling points sparse, which could lead to an insufficient representation of greenery within the area, resulting in biases such as distance-perspective limitations and proximity amplification. The spatial sampling scope of street view is limited, further leading to biases associated with access limitations. For instance, GSV primarily covers major urban roads and often fails to capture significant green areas within many street blocks, such as football fields, private gardens, and parks. It is also worth noting that GSV's sampling rarely extends to urban peripheries and covers only about a hundred countries, not the entire globe. Additionally, the temporal resolution of street view sampling is another major source of bias. However, the emergence of new sampling devices, such as the increasing use of smaller data collection vehicles like electric bicycles in neighborhoods and parks in China, may reduce biases related to access limitations. Moreover, the integration of official street view data from platforms like Google Maps and Baidu Map with crowdsourced street view data such as Mapillary may help alleviate issues of sparse sampling points.

With the intensification of urbanization and the emergence of new vertical greenery elements [34,35], the challenges for satellite-based urban greenery measurements are also increasing. The commonly used Sentinel-2 images have a spatial resolution of only 10 m, which makes it challenging to conduct finer greenery measurements. Moreover, current conventional optical sensors struggle to penetrate tree canopies and are frequently obstructed by cloud cover, causing biases such as multi-layer greenery concealment and noise. However, the gradual widespread adoption of new sensors is expected to provide satellite imagery with higher spatiotemporal resolutions, and the use of technologies like radar enhances penetration capabilities. These new technologies could help mitigate biases to some extent.

Since satellite and street view imagery each capture different aspects of urban greenery [23,36], integrating these two sources may provide a representation close to the "true" state of urban greenery.

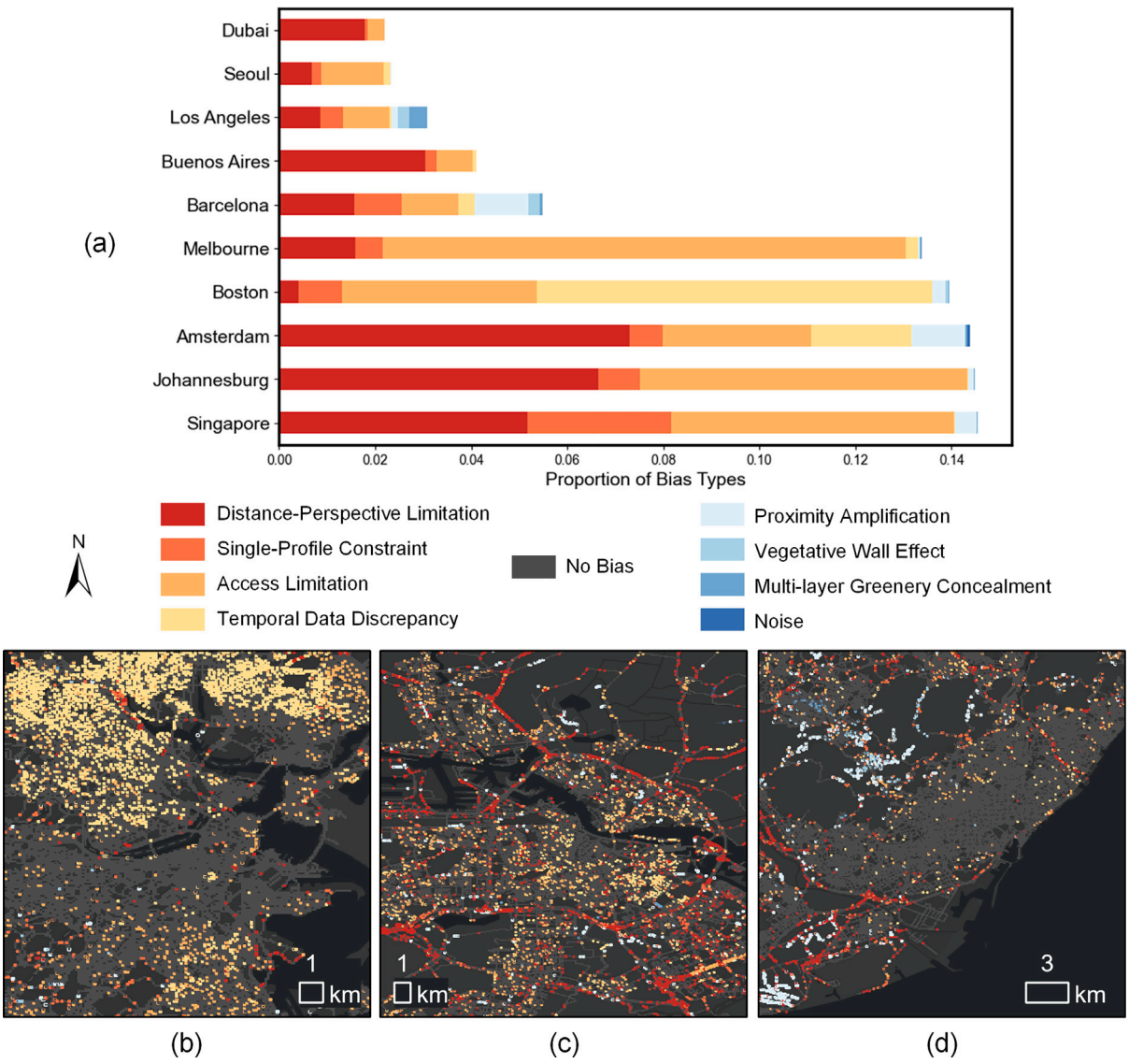

Fig. 7. Quantification of bias types. (a) Proportional distribution of different bias types across ten cities; (b) Spatial distribution of bias types in Boston; (c) Spatial distribution of bias types in Amsterdam; (d) Spatial distribution of bias types in Barcelona.

Numerous studies have already explored the fusion of satellite and street view imagery to more comprehensively characterize urban environments, and this approach is equally applicable to urban greenery. For instance, some research has proposed using the ratio of NDVI to GVI as a new index to indicate the intensity of greenery in the vertical space [18]. Other methods of integration remain a promising area for future research.

4.2. Implications for urban design and planning

First, we highlight the main factors that contribute to the biases in urban greenery measurements. Given the significance of urban greenery in cities, it is crucial to acknowledge potential risks associated with utilizing biased urban greenery data as a basis for guiding urban design and planning decisions. For instance, relying solely on street view-based urban greenery to determine locations for adding green spaces may lead to erroneous decisions due to factors such as distant or nearby greenery, which could impact the overall effectiveness of such interventions.

Second, the detailed analysis of the two measurements in describing urban greenery offers valuable insights for urban design and planning optimization. Leveraging the disparities between the two measurements, urban planners can identify potential areas of inaccessible greenery. Consequently, policies such as the removal of unnecessary fences and other barriers can be implemented to enhance public access to urban greenery. These findings can serve as valuable guidance for urban design and planning practices to enhance the overall quality and accessibility of urban green spaces.

4.3. Study limitations and future challenges

Although this study trained a machine learning model to detect bias across broad urban areas, the model's accuracy is not particularly high. One contributing issue is the significant imbalance in the data, as seen in Table 2, where the number of samples in the "noise" category is very small. This scarcity likely makes it difficult for the model to effectively learn the characteristics of this type of bias. Additionally, the machine learning method employed is relatively simple, and the feature extraction models are primarily designed for urban scene recognition. As a result, it may not capture the distinctions between different types of bias effectively. Future approaches, such as using self-supervised or semi-supervised learning methods, may better enable the model to extract bias-related features. Moreover, bias may result from a combination of multiple factors, making it difficult even for humans to

determine the primary factor. This complexity, driven by the urban environment and the data collection methods, presents a significant challenge for the automated detection of bias risk. Furthermore, the model's performance may vary across different regions or city types due to factors such as climate, urban density, and greenery typologies. However, exploring these regional differences requires additional data, including detailed climate information and urban morphological characteristics across a larger number of cities, as well as significantly more extensive annotation work. In future work, expanding the dataset to include more cities from diverse climatic zones and urban forms would enable a more comprehensive assessment of the model's effectiveness in different contexts.

5. Conclusion

In summary, this study underscores the complexities and inherent biases associated with measuring urban greenery through satellite and street view imagery. By systematically identifying eight main factors contributing to these biases, we have highlighted the discrepancies between NDVI and GVI measurements across various global cities. The quantification of bias types and their spatial distributions provides a nuanced understanding of how these factors manifest in different urban environments. These insights are crucial for urban planners and policymakers aiming to enhance the accuracy of urban greenery assessments, which are vital for sustainable urban development and improving the quality of life for city residents.

The research also opens avenues for future work, including the development of advanced methodologies to reduce measurement biases and the exploration of additional data sources. As cities continue to grow and evolve, the need for precise and comprehensive greenery measurements becomes increasingly important, necessitating continuous advancements in technology and methodology. This study provides a foundation for such future explorations and contributes to the broader discourse on urban sustainability and environmental planning.

CRediT authorship contribution statement

Yingjing Huang: Writing – review & editing, Writing – original draft, Visualization, Validation, Methodology, Formal analysis, Data curation. **Rohit Priyadarshi Sanatani:** Writing – original draft, Methodology, Data curation. **Chang Liu:** Methodology, Formal analysis, Data curation. **Yuhao Kang:** Validation, Methodology, Data curation. **Fan Zhang:** Writing – review & editing, Validation, Supervision, Resources. **Yu Liu:** Writing – review & editing, Supervision. **Fabio Duarte:** Validation, Supervision, Project administration, Conceptualization. **Carlo Ratti:** Supervision, Project administration.

Declaration of competing interest

The authors declare that they have no known competing financial interests or personal relationships that could have appeared to influence the work reported in this paper.

Acknowledgment

The authors would like to thank the financial support received from the members of the Senseable City Lab consortium, including the AMS Institute, Dubai Future Foundation, Arnold Ventures, Toyota, UnipolTech, Consiglio per la Ricerca in Agricoltura e l'Analisi dell'Economia Agraria, Tele2, Volkswagen Group America, FAE Technology, Fédération Internationale de l'Automobile, Amsterdam and Rio de Janeiro. This work was also supported by the High-performance Computing Platform of Peking University. We thank all members of MIT Senseable City for their comments.

Data availability

The analysis was conducted using Python. Data and code used in this study is publicly accessible via the Zenodo repository at https://doi.org/10.5281/zenodo.13167483.

References

[1] S. Lee, Does tree canopy moderate the association between neighborhood walkability and street crime? Urban Forestry Urban Greening 65 (2021) 127336.
[2] J. Zhang, S. Zhou, T. Xia, Y. Yin, X. Wang, Y. Cheng, Y. Mao, B. Zhao, Residential greenspace exposure, particularly green window-views, is associated with improved sleep quality among older adults: Evidence from a high-density city, Build. Environ. 253 (2024) 111315.
[3] M. Viecco, S. Vera, H. Jorquera, W. Bustamante, J. Gironás, C. Dobbs, E. Leiva, Potential of particle matter dry deposition on green roofs and living walls vegetation for mitigating urban atmospheric pollution in semiarid climates, Sustainability 10 (7) (2018) 2431.
[4] C.P. Loughner, D.J. Allen, D.-L. Zhang, K.E. Pickering, R.R. Dickerson, L. Landry, Roles of urban tree canopy and buildings in urban heat island effects: parameterization and preliminary results, J. Appl. Meteorol. Climatol. 51 (10) (2012) 1775–1793.
[5] H. Bobál'ová, A. Benová, M. Kožuch, Hierarchical object-based mapping of urban land cover using sentinel-2 data: A case study of six cities in central europe, PFG–J. Photogrammetr. Remote Sens. Geoinformat. Sci. 89 (2021) 15–31.
[6] X. Zhang, P. Song, Estimating urban evapotranspiration at 10 m resolution using vegetation information from sentinel-2: A case study for the Beijing sponge city, Remote Sens. 13 (11) (2021) 2048.
[7] J. Rouse Jr., R. Haas, J. Schell, D. Deering, Monitoring vegetation systems in the great plains with erts, in: Third Earth Resources Technology Satellite-1 Symposium: Section AB. Technical Presentations, 1, Scientific and Technical Information Office, National Aeronautics and Space ..., 1974, p. 309.
[8] R.P. Sripada, R.W. Heiniger, J.G. White, A.D. Meijer, Aerial color infrared photography for determining early in-season nitrogen requirements in corn, Agron. J. 98 (4) (2006) 968–977.
[9] Y. Xiang, C. Yuan, Q. Cen, C. Huang, C. Wu, M. Teng, Z. Zhou, Heat risk assessment and response to green infrastructure based on local climate zones, Build. Environ. 248 (2024) 111040.
[10] B.Y. Cai, X. Li, I. Seiferling, C. Ratti, Treepedia 2.0: applying deep learning for large-scale quantification of urban tree cover, in: 2018 IEEE International Congress on Big Data (BigData Congress), IEEE, San Francisco, CA, 2018, pp. 49–56.
[11] F. Biljecki, T. Zhao, X. Liang, Y. Hou, Sensitivity of measuring the urban form and greenery using street-level imagery: A comparative study of approaches and visual perspectives, Int. J. Appl. Earth Obs. Geoinf. 122 (2023) 103385.
[12] Y. Kang, F. Zhang, S. Gao, H. Lin, Y. Liu, A review of urban physical environment sensing using street view imagery in public health studies, Ann. GIS 26 (3) (2020) 261–275.
[13] J. Yang, L. Zhao, J. Mcbride, P. Gong, Can you see green? Assessing the visibility of urban forests in cities, Landsc. Urban Plan. 91 (2) (2009) 97–104.
[14] Y. Han, T. Zhong, A.G. Yeh, X. Zhong, M. Chen, G. Lü, Mapping seasonal changes of street greenery using multi-temporal street-view images, Sustainable Cities Soc. 92 (2023) 104498.
[15] Y. Hu, F. Qian, H. Yan, A. Middel, R. Wu, M. Zhu, Q. Han, K. Zhao, H. Wang, F. Shao, Z. Bao, Which street is hotter? Street morphology may hold clues -thermal environment mapping based on street view imagery, Build. Environ. 262 (2024) 111838.
[16] K. Mihara, D.J.C. Hii, H. Takasuna, K. Sakata, How does green coverage ratio and spaciousness affect self-reported performance and mood? Build. Environ. 245 (2023) 110939.
[17] L. Ji, C. Shu, A. Gaur, L. Wang, M. Lacasse, A state-of-the-art review of studies on urban green infrastructure for thermal resilient communities, Build. Environ. 257 (2024) 111524.
[18] A. Larkin, P. Hystad, Evaluating street view exposure measures of visible green space for health research, J. Exposure Sci. Environ. Epidemiol. 29 (4) (2019) 447–456.
[19] J. Torkko, A. Poom, E. Willberg, T. Toivonen, How to best map greenery from a human perspective? Comparing computational measurements with human perception, Front. Sustain. Cities 5 (2023) 1160995.
[20] Y. Kumakoshi, S.Y. Chan, H. Koizumi, X. Li, Y. Yoshimura, Standardized green view index and quantification of different metrics of urban green vegetation, Sustainability 12 (18) (2020) 7434.
[21] M. Helbich, R. Poppe, D. Oberski, M. Zeylmans van Emmichoven, R. Schram, Can't see the wood for the trees? An assessment of street view- and satellite-derived greenness measures in relation to mental health, Landsc. Urban Plan. 214 (2021) 104181.

[22] M. Tong, J. She, J. Tan, M. Li, R. Ge, Y. Gao, Evaluating street greenery by multiple indicators using street-level imagery and satellite images: a case study in nanjing, China, Forests 11 (12) (2020) 1347.
[23] R. Wang, M. Helbich, Y. Yao, J. Zhang, P. Liu, Y. Yuan, Y. Liu, Urban greenery and mental wellbeing in adults: Cross-sectional mediation analyses on multiple pathways across different greenery measures, Environ. Res. 176 (2019) 108535.
[24] Y. Lu, Y. Yang, G. Sun, Z. Gou, Associations between overhead-view and eye-level urban greenness and cycling behaviors, Cities 88 (2019) 10–18.
[25] D. Moravec, J. Komárek, S. López-Cuervo Medina, I. Molina, Effect of atmospheric corrections on NDVI: Intercomparability of landsat 8, sentinel-2, and UAV sensors, Remote Sens. 13 (18) (2021) 3550.
[26] G. Boeing, OSMnx: New methods for acquiring, constructing, analyzing, and visualizing complex street networks, Comput. Environ. Urban Syst. 65 (2017) 126–139.
[27] R. Ranftl, A. Bochkovskiy, V. Koltun, Vision transformers for dense prediction, 2021, arXiv:2103.13413.
[28] D.N. Gonçalves, J. Marcato, A.C. Carrilho, P.R. Acosta, A.P.M. Ramos, F.D.G. Gomes, L.P. Osco, M. da Rosa Oliveira, J.A.C. Martins, G.A. Damasceno, M.S. de Araújo, J. Li, F. Roque, L. de Faria Peres, W.N. Gonçalves, R. Libonati, Transformers for Mapping Burned Areas in Brazilian pantanal and amazon with PlanetScope imagery, Int. J. Appl. Earth Obs. Geoinf. 116 (2023) 103151.
[29] B. Zhou, H. Zhao, X. Puig, S. Fidler, A. Barriuso, A. Torralba, Scene parsing through ADE20k dataset, in: 2017 IEEE Conference on Computer Vision and Pattern Recognition, CVPR, IEEE, Honolulu, HI, 2017, pp. 5122–5130.
[30] X. Li, C. Zhang, W. Li, R. Ricard, Q. Meng, W. Zhang, Assessing street-level urban greenery using Google Street View and a modified green view index, Urban Forestry Urban Greening 14 (3) (2015) 675–685.
[31] A. Getis, J.K. Ord, The analysis of spatial association by use of distance statistics, Geograph. Anal. 24 (3) (1992) 189–206.
[32] Z. Zhang, T. Zhao, Y. Guo, J. Yin, RS5M: A large scale vision-language dataset for remote sensing vision-language foundation model, 2023, arXiv:2306.11300.
[33] B. Zhou, A. Lapedriza, A. Khosla, A. Oliva, A. Torralba, Places: A 10 million image database for scene recognition, IEEE Trans. Pattern Anal. Mach. Intell. (2017).
[34] M. De Groeve, E. Kale, S. Godts, S.A. Orr, T. De Kock, Impact of vertical greening on urban microclimate and historic building materials: A meta-analysis, Build. Environ. 253 (2024) 111365.
[35] Y. Zhou, J. Chen, D. Wei, Z. Zhang, Research on relationship between the thermophysical parameters of green facade and leaf area index (LAI), Build. Environ. 260 (2024) 111663.
[36] I.A.V. Sánchez, S.M. Labib, Accessing eye-level greenness visibility from open-source street view images: A methodological development and implementation in multi-city and multi-country contexts, Sustainable Cities Soc. 103 (2024) 105262.